REVIEW ARTICLE

Physico-chemical properties of double porous scaffolds of polycaprolactone/chitosan and graphene nano scrolls

Article history:
Received: 10-09-2023
Revised: 08-12-2023
Accepted: 14-12-2023

Lillian Mambiri[a], Gabrielle Broussard[b], Tahsin Zaman[c], Dilip Depan[d]

Abstract: The use of graphene-based nanomaterials in tissue engineering has shown immense potential in improving the microstructure of polymeric blends. The addition of graphene nanoscrolls (GNS) to polycaprolactone (PCL) and chitosan (CHT) scaffolds and the subsequent improvements in physical properties, crystallinity, and degradation rate are indeed promising. The use of techniques like DSC (differential scanning calorimetry) and XRD (x-ray diffraction) to characterize thermal behavior and crystal state provides valuable insights into the material properties. FTIR spectroscopy demonstrated the changes in the chemical structure of the polymer blend during degradation, while nanoindentation was used to study the mechanical properties of the scaffolds. The SEM (scanning electron microscopy) images offering a closer look at the surface morphology and microstructure further contribute to a comprehensive understanding of the scaffold's characteristics. The enhanced crystallinity and lower degradation rate, coupled with a well-defined interconnected pore structure, suggest that the integration of graphene nanoscrolls at a concentration of 0.1 wt.% is a beneficial approach. This not only improves the material properties but also creates an optimal environment for potential tissue engineering applications, particularly for load-bearing tissues.

Keywords: Polycaprolactone; Chitosan; Graphene nanoscrolls; Degradation; Double porosity.

[a] Institute for Materials Research and Innovation, Chemical Engineering Department, University of Louisiana at Lafayette, P.O. Box 44130, Lafayette, LA 70504-4130, USA.

[b] Institute for Materials Research and Innovation, Chemical Engineering Department, University of Louisiana at Lafayette, P.O. Box 44130, Lafayette, LA 70504-4130, USA.

[c] Laboratory of Composite Materials, Mechanical Engineering Department, University of Louisiana at Lafayette, P.O. Box 43678, Lafayette, LA 70504.

[d] Institute for Materials Research and Innovation, Chemical Engineering Department, University of Louisiana at Lafayette, P.O. Box 44130, Lafayette, LA 70504-4130, USA. Corresponding author: ddepan@louisiana.edu

INTRODUCTION

Tissue engineering has led to several innovations in regenerative medicine and disease modeling (Ashammakhi *et al.*, 2022). The development of three-dimensional scaffolds that encourage cell adhesion and proliferation has been a significant focus in tissue engineering research (Loh & Choong, 2013; Sun *et al.*, 2021). Despite the numerous advancements, tissue engineering still has a slew of unresolved issues, such as the necessity of improved biomaterial designs and the constraints of successful application due to inadequate mechanical integrity (Bonithon *et al.*, 2021). For scaffolds to be successful in their applications, they must have an array of properties, such as porosity for nutritional and oxygen passage and waste elimination, as well as adequate mechanical integrity to withstand physiological conditions (Parisien *et al.*, 2022).

Porosity and pore size are critical factors that affect the functionality of biomedical 3D scaffolds. A porous microstructure with

appropriate porosity is typically required for tissue integration and growth (Das *et al.*, 2019). A porous network is essential in promoting and directing the growth of new tissue. Greater porosity enhances bone growth, fluid flow, nutrient, and oxygen access, and facilitates the removal of cell debris (Cheng *et al.*, 2018). In addition, the material of the scaffold is equally important for its intended application. Polymeric scaffolds and composites are highly sought after for tissue engineering applications due to their ability to be customized and tailored for specific properties (Basavegowda & Baek, 2021). Synthetic polymers such as polyester, polycaprolactone (PCL), poly (lactic-co-glycolic acid) (PLGA), polylactic acid (PLA), and polyurethane (PU) are favored for their biocompatibility, biodegradability, and mechanical strength (Bartnikowski *et al.*, 2019).

PCL is highly favored for scaffolds due to its high toughness, elasticity, and controlled degradation rates (Kao *et al.*, 2022). The hydrophobicity of PCL has resulted in the development of novel nanocomposites with tailored degradation rates and improved physico-chemical properties (Ferroni *et al.*, 2022). Blending natural polymers such as chitosan (CHT) can improve the mechanical properties of the scaffold and provide a favorable environment for cell attachment (Islam *et al.*, 2020). Natural polymers are cost-effective but highly sensitive to water, making it crucial to enhance their mechanical qualities for tissue engineering scaffolds (Depan *et al.*, 2011). Weak scaffolds may harm cells and impede tissue formation, requiring careful consideration of materials, design, and manufacture (Depan *et al.*, 2011). While blending with natural polymers such as CHT can improve the mechanical properties, its water sensitivity can weaken the blend, thereby affecting cell growth and tissue formation (Depan *et al.*, 2011).

However, the inherent poor processability of CHT limits its applications in blends with other polymers, especially as a tissue engineering porous scaffold. PCL, on the other hand, displays high miscibility with CHT, thereby improving its usage and processability. PCL, being a hydrophobic and semicrystalline polymer, with less functionality poses challenges in various applications. Moreover, high melting (60-64 ºC) with low glass transition temperature (-60 ºC) render high toughness under physiological conditions, with slower degradation rates than natural biopolymers. The mechanical properties, biodegradability, and biocompatibility of the pure PCL aren't enough with the requirements for some of the applications such as bone tissue engineering. For that reason, PCL can also be used as one of the blend components of biomaterials or as a copolymer (Mondal *et al.*, 2016).

Tissue engineering polymeric scaffolds face challenges such as inadequate mechanical strength. One potential solution is to employ carbon-based nanoparticles such as graphene which possess versatile properties such as chemical stability, thermal and electrical conductivity, and mechanical strength (Ajala *et al.*, 2019). These properties can be modified through chemical and physical methods to produce related materials like single and multilayered graphene, graphene oxide, and reduced graphene oxide (Ajala *et al.*, 2019).The study focuses on the use of graphene nanoscrolls (GNSs) that have open morphologies and two opposing energy contributions that determine scroll growth (Ajala *et al.*, 2019).

While the use of graphene has been studied in drug delivery and tissue engineering applications, no studies have explored the effect of GNSs on the mechanical strength of a porous polymer matrix. The study's exploration of using GNSs as a reinforcement material for a biodegradable polymer matrix has important implications for developing scaffolds with improved properties while supporting cell growth and tissue regeneration addresses a critical need in tissue engineering. The objective of this work is to create a biodegradable 3D porous scaffold material with interconnected microporosities. The study used a 90/10 PCL/CHT blend with a specific weight fraction of GNSs to investigate chemical interactions, biodegradability, and swelling behavior. The prepared formulation will have potential applications in tissue engineering, drug delivery, artificial vascular grafts, biodegradable implants, and regenerative engineering of various tissues and organs.

MATERIALS

Chitosan (CHT), acetic acid, formic acid, sodium hydroxide, and lysozyme were purchased from Sigma-Aldrich, Milwaukee, USA. Polycaprolactone (PCL) was purchased from Perstorp Holding AB, Sweden. Isopore® Polyester (PET) track-etched membranes (with 10 μm pore diameter), used as macro void generators, were purchased from Sterlitech, USA. Phosphate buffer saline (PBS) was purchased from Fisher Scientific, USA.

PREPARATION OF GNS-LOADED PCL AND CHT (PCSG) MEMBRANES

GNS was prepared as per our previous report.[15] Briefly, 1.0 mg of GNPs were added to 10 mL of toluene and sonicated, followed by immersion into liquid nitrogen. Next, the frozen toluene was allowed to melt at room temperature, thereby separating GNS after complete solvent evaporation. This method provides highly stable GNS with excellent reproducibility. The membranes were developed by a solvent casting method as shown in Fig 1, using a formic acid/acetic acid (FA/AA) mixture as a solvent and NaOH aqueous solution as a non-solvent (Das *et al.*, 2019, 2020). PCL and CHT at a ratio of 90:10 were dissolved in 60:40 formic acid/acetic acid with GNS concentrations of 0% and 0.1%. Samples were named PCSG0.0 and PCSG10.0, respectively as shown in Table 1.

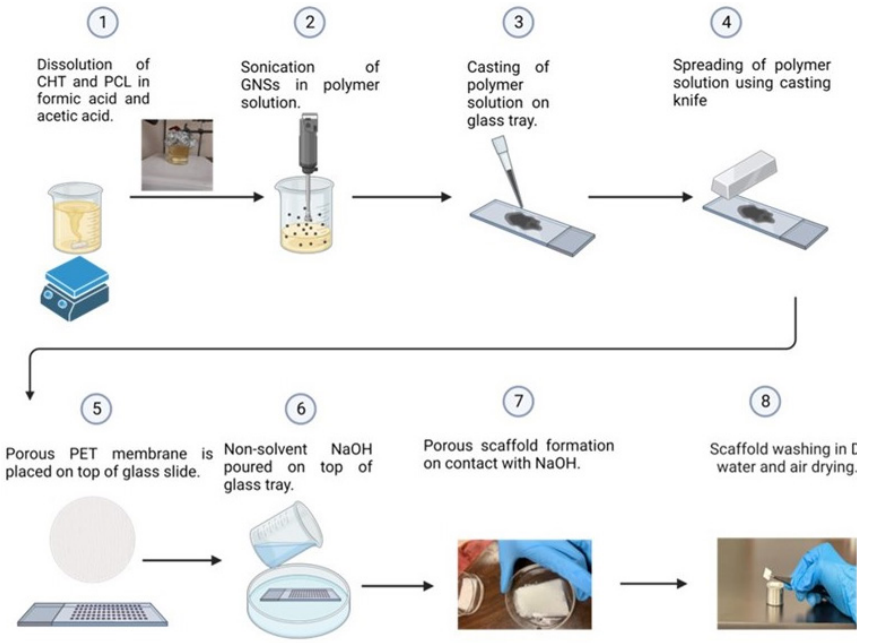

Figure 1. Schematic illustration of the steps utilized in the formation of PCL/CHT/GNS scaffolds with double porosity fusing track-etched membranes.

Sample name	GNS wt. %	Pore Diameter (μm)	Porosity (%)	Crystallinity (%)
PCSG0.0	0	10.3	65.7	58.6
PCGS10.0	0.1	10.3	66.6	61.1

Table 1. Summary of the polymer blend membrane properties pore diameter, and porosity.

The polymer solution was cast on a glass plate at 25 ºC. CHT was dissolved in a formic acid and acetic acid mixture for 12 hours at 55 ºC. After the CHT had fully dissolved and the solution was of a clear thick viscous yellow solution, it was allowed to cool down to 35 ºC. PCL was added at that point and allowed to dissolve for 2 hours.

The polymeric solution was further cooled down to 25 ºC and graphene nanoscrolls (GNSs) were added to the solution. GNSs were synthesized as per our prior report (Ajala *et al.*, 2019). The GNSs were then dispersed with a probe sonicator for 10 minutes with 30-second pauses in between sonication. The polymer composite was cast on a glass tray and uniformly spread to a thickness of 250 μm using a casting knife. The membrane was soaked in a formic acid and acetic acid mixture, and excess acid was removed and carefully placed on top of the spread polymer solution. The tray was gently immersed in 1 M solution of sodium hydroxide, and the membrane began to form immediately. The membranes detached from the glass tray after the track-etched membrane was removed gently and the newly formed membranes were washed several times in pure water. Then, the membranes were stored in deionized water at 4 ºC.

FABRICATION OF DOUBLE POROUS PCSG SCAFFOLDS

Membranes were developed using a solvent casting method with a formic acid/acetic acid (FA/AA) mixture as a solvent and NaOH aqueous solution as a non-solvent. The polymer solution was composed of PCL and CHT at a ratio of 90:10 dissolved in a 60:40 formic acid/acetic acid solution, with GNS concentrations of 0% and 0.1% for samples named PCSG0.0 and PCSG10.0, respectively. The process involved dissolving CHT in the formic acid and acetic acid mixture for 12 hours at 55 ºC. After complete dissolution, the solution was left to cool down to 35 ºC, PCL was added to the cooled CHT solution and allowed to dissolve for 2 hours. Once the PCL had dissolved, the polymer solution was left to cool down to 25 ºC. Upon cooling down to 25 ºC, graphene nanoscrolls (GNSs) were added to the polymer solution. The GNSs were dispersed in the polymer solution using a probe sonicator for 10 minutes with 30-second pauses to maintain a temperature of 25 ºC. The sonicated GNS-polymer solution was cast on a glass tray, and spread uniformly to a thickness of 250 µm using a casting knife. The tray was gently immersed in a 1 M solution of sodium hydroxide, and the membrane began to form immediately. After detaching from the glass tray, the newly formed membrane was washed several times in pure water and stored in deionized water at 4 ºC.

The solvent casting technique involves dissolving a blend of PCL and CHT polymers in a mixture of formic acid and acetic acid solvents (Das *et al.*, 2019, 2020). Upon adding sodium hydroxide as a non-solvent to the solution, the polymer blend precipitates out, yielding a dual-porous structure characterized by interconnected pores. This fabrication process results in double porous PCSG scaffolds.

The first degree of porosity, on the top surface, is created by the formation of pores within the polymer matrix due to the evaporation of the acetic acid and formic acid (Das *et al.*, 2019, 2020). The second degree of porosity is created by the formation of larger pores caused by the precipitation of the polymer induced by NaOH (Das *et al.*, 2019, 2020).

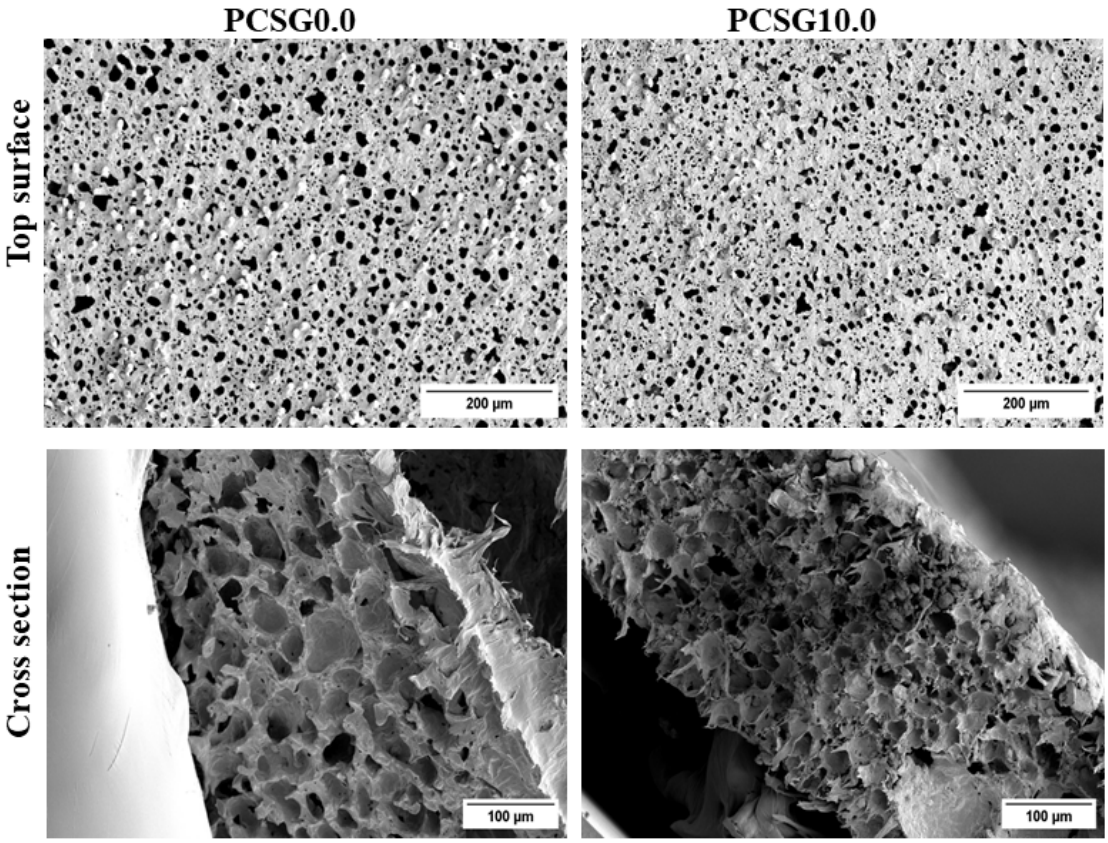

Figure 2. Scanning electron micrographs of cross-section and top surface of PCSG scaffolds after fabrication.

PCL and CHT are used in scaffold fabrication to create a biocompatible and biodegradable matrix as shown in Fig.2. Das *et al.* investigated the range of chemical interactions, miscibility, and biodegradability by varying the percentage ratios of PCL/CHT (100/0, 90/10, 80/20, 70/30 w/w %). It was concluded that at higher concentrations of CHT, porosity increases resulting in increased degradation rates therefore scaffolds fabricated with a ratio of PCL/CHT (90/10 wt.%) had superior mechanical integrity and exhibited better degradation control and better mechanical properties, therefore, the ratio 90/10 wt.% was used for this study. Incorporating GNSs into the scaffold can further augment its mechanical and electrical characteristics. Due to their high surface area, GNSs can improve mechanical strength by increasing crystallinity which in turn results in increased Young's modulus (Ajala *et al.*, 2019; Shin *et al.*, 2016).

CHARACTERIZATION TECHNIQUES

Scanning electron microscopy (SEM) was used to analyze the surface morphology for the double porosity membranes at an accelerating voltage of 5 kV. The average pore diameter of the macro-voids and micropore size distribution were evaluated using the microscope. The porosity was measured using Image J software. Images of both the cross-section and the top of the samples were taken. Samples were mounted on aluminum stubs using carbon tape and were sputter coated with a layer of gold with a thickness of 12 nm before imaging.

The dry scaffolds were weighed. Then, the scaffolds were immersed in phosphate-buffered saline (PBS) at pH 7.4 at 37 ºC for 24 hours. After 24 hours, the scaffolds were removed and wiped with blotting paper to remove any adsorbed water. The wet weights of the scaffolds were taken. The ratio of swelling was determined using the following formula:

$$\frac{W_f - W_i}{W_i} \times 100 = W_{swelling} \quad (1)$$

W_i = *Initial weight*

$W_{swelling}$ = *Swelling weight percentage*

W_f = *Final weight*

Enzymatic degradation of the membrane was studied using lysozyme. The initial dry weight of the samples (Wi) was recorded followed by incubating in the degradation media for hydrolysis (0.1 M PBS containing 500 µg ml^{-1} of lysozyme at 37 ºC) in an incubator. The membrane was taken out from the degradation media, washed with distilled water, and weighed, while the extent of degradation was quantified as the change in sample weight over time. The percentage of weight loss was given by:

$$\frac{W_i - W_f}{W_i} \times 100 = W_{loss} \quad (2)$$

W_i = *Initial weight*

W_{loss} = *Weight loss percentage*

W_f = *Final weight*

Bruker Lumos II Fourier transform infrared radiation (FTIR) was used for chemical analysis. Samples were evaluated with the reflectance sampling technique under attenuated total reflectance (ATR) mode. Each point was scanned 16 times with a resolution of 8 cm^{-1}.

The thermal behavior of the PCSG membranes was tested using Perkin Elmer 4000 differential scanning calorimetry (Shelton, CT, USA). Samples were freeze-dried and then crushed into a fine powder weighed to 15-20 mg and then placed into aluminum pans. Samples were heated from 20 ºC to 120 ºC at a rate of 5 ºC/min, then held isothermally for 5 minutes to erase thermal history. They were cooled to –10 ºC. Nitrogen was used as the purge gas at a flow rate of ~20 ml/min. Experiments were conducted in triplicates.

The mechanical properties of the scaffolds were determined from load-displacement curves obtained with an MTS Nano indenter XP apparatus. Nanoindentation tests with continuous stiffness measurement (CSM) were carried out for indentation modulus measurements. All experiments were performed with a diamond-type Berkovich indenter. The strain rate and the frequency oscillation of the displacement varied in the range of 0.01-0.2 s^{-1} and 1-45 Hz, respectively. The parameters set for the measurement are a depth of 2 µm and an amplitude of 2 nm. Each value was computed as an average of 20 measurements in the range of 0-2000 nm penetration depth.

The experimental results were presented in the form of mean values accompanied by standard error (SE) for each group of samples. Each experiment was conducted with a minimum of three replicates to ensure scientific validity.

RESULTS AND DISCUSSION

After scaffold preparation, the top surface, and the cross-section morphological characteristics

were observed in SEM. All the scaffolds showed double porosity where the macro voids are open towards the top surface and connected with the spongy microporous network. Fig. 2 shows the top surface of the scaffold, illustrating the formation of circular pores of diameter 10 µm in all samples due to the evaporation of the acid solvent. From the cross-section view (bottom Fig. 2), it was observed that the localized arrival of the sodium hydroxide inside the polymer solution resulted in macro void pores with diameters of 21.7 µm, and 6.3 µm for PCSG0.0, and PCSG10.0, respectively. The porosity of the scaffolds (Table 1) was analyzed by ImageJ Analysis software and recorded as 65.7 %, and 66.6% for PCSG0.0, and PCSG10.0, respectively.

Ratios of PCL and CHT were kept constant at 90/10 therefore no difference was observed in the pore diameter, indicating that GNSs did not have any effect on pore size or pore interconnectivity after fabrication. However, the porosity was moderately different in the two scaffolds due to the presence of GNSs which inhibited the formation of more pores. In solvent casting, the polymer solution undergoes phase inversion, which refers to the transition of a polymer solution from a homogeneous phase (polymer and solvent) to a porous phase, where the solvent evaporates, and pores are formed (Das *et al.*, 2020; Lanjewar *et al.*, 2020). Therefore, it is said that the phenomenon of pore formation is due to the thermodynamics of the solution and kinetics of the phase inversion mechanism (Lanjewar *et al.*, 2020; Matsuda, 1991). However, when nanoparticles are added to a polymer solution, they affect the phase inversion kinetics by acting as physical barriers that disrupt the formation of pores (Lanjewar *et al.*, 2020; Matsuda, 1991). Since GNSs are technically in the solid state, they slow down the phase inversion process which in turn results in lower porosity. However, notably, GNS may act as a lubricant and may decrease the viscosity of the polymer blend, resulting in increased pore size during solvent evaporation. The lower amount of GNS in our case did not impart this scenario but illustrated that by varying the amount of GNS, an optimal pore size and porosity can be achieved.

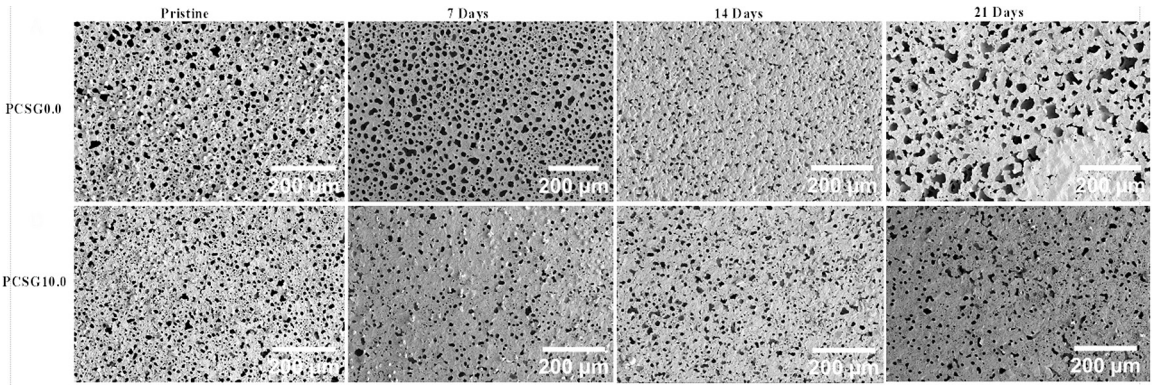

Figure 3. Scanning electron micrographs of the top surface, before and after *in vitro* enzymatic degradation.

For this study, a circular track-etched membrane was used to control the geometry of the pores. Generally, circular pores are widely used in tissue engineering because they are quite easy to produce and offer homogeneous mechanical characteristics throughout the scaffold. The pore size shown in (Fig 3) was observed and summarized in Table 2 after enzymatic degradation over 21 days at 7-day intervals. PSCG0.0 exhibited an increase in pore size going from 10.3 µm to 17.2 µm. The pore diameter increased, over the 21 days, as more lysozyme was diffused into the matrix, resulting in the collapsing of the pores. On the other hand, PCSG10.0 had no notable change in pore size going from 10.3 µm to 11.2 µm which indicates that at concentrations of 0.1 wt.% GNS, degradation was slower. Table 3 shows that enzymatic degradation after 21 days of PCSG0.0, and PCSG10.0 had an average weight loss of 5.7 %, and 2.60 % respectively.

Circular pores possess higher porosity than other geometries and are highly effective in nutrient diffusion for bone tissue engineering applications. Further, circular pores with high porosity can not

	Pore Diameter Pristine μm	Pore Diameter Day 7 μm	Pore Diameter Day 14 μm	Pore Diameter Day 21 μm
PCSG0.0	10.3	10.9	13.8	17.2
PCSG10.0	10.3	10.4	10.4	11.2

Table 2. Pore diameter after *in vitro* enzymatic degradation.

	Day 1	±	Day 7	±	Day 14	±	Day 21	±
PCSG0.0	7.7%	2.7	6.7%	3.2	11.3%	3.1	5.7%	1.9
PCSG10.0	8.5%	6.0	8.9%	5.0	9.8%	0.5	2.6%	1.0

Table 3. Average percent weight loss of scaffolds during *in vitro* degradation.

only facilitate protein adsorption and bone healing but also resemble the compressive strength of natural bone.[25] So, GNS, when added with PCL and CHT provides a balance to the compromised stiffness in the original configuration.

The choice of material can have significant effects on the rate of enzymatic degradation. Enzymes are quite specialized in how they work and can only break down specific kinds of molecules. Typically, PCL degrades in lysozyme through hydrolysis. By targeting the carbonyl group in the ester linkage, lysozyme attaches to the PCL chain and cleaves the ester bonds, resulting in the production of an alcohol and a carboxylic acid (Abdelfatah *et al.,* 2021; Bartnikowski *et al.,* 2019). Lysozyme can also break down the biopolymer CHT, which is made up of glucosamine and N-acetylglucosamine units (Depan *et al.,* 2011). This is achieved through hydrolyzing the β-1,4 glycosidic links between the glucosamine and N-acetylglucosamine units (Aranaz *et al.,* 2021; Kean & Thanou, 2010). The presence of GNS may have played a role in lowering the rate of degradation for this scaffold. This behavior could be attributed to the difficulty for the enzymes to reach the bulk matrix due to the nanoparticles' barrier properties that make the diffusion path more tortuous (Biscaia *et al.,* 2022; Castilla-Cortázar *et al.,* 2019). This weight loss in (Fig.4a) shows that tailoring the concentration of GNS in the scaffolds may assist in lowering undesirable bulk degradation if an optimal concentration can be determined. Long-term functionality of tissue-engineered cell-material constructs depends on enzymatic biodegradation activity. CHT generally degrades faster than PCL owing to low crystallinity and hydrophilicity. The degraded CHT might leach out from the pores creating larger pores and giving access to the diffusion of the enzymes deeper into the bulk of the sample. Once the enzyme adsorbs on the polymer surface, it tends to form an enzyme-matrix complex, followed by enzyme-catalyzed degradation. The enzyme can also form fibrillar aggregates on the surface (Luyt & Kelnar, 2019; Wu *et al.,* 2011).

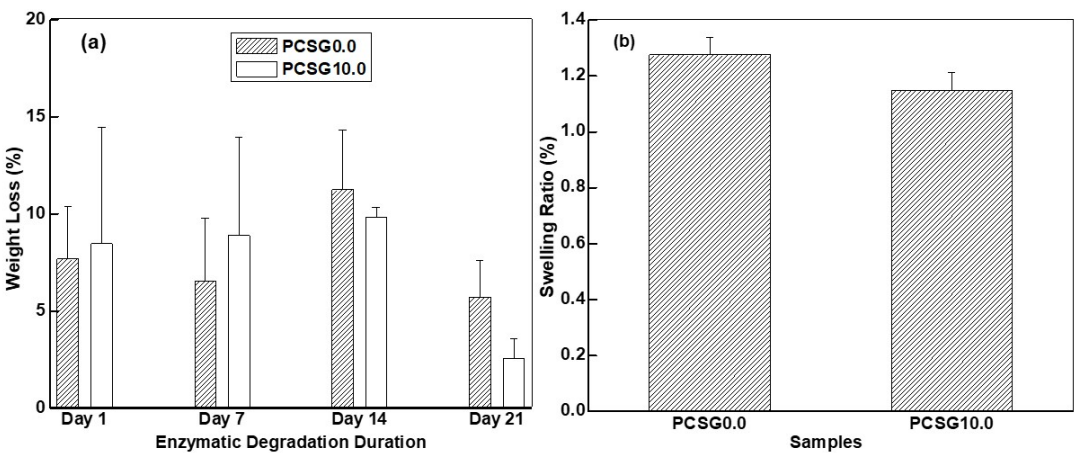

Figure 4. a) Weight loss concerning duration of enzymatic degradation, b) Swelling ratios after 24 hours of immersion in PBS.

After 24 hours of immersion in PBS, pH 7.4 and 37 ºC, swelling studies showed that the addition of GNS may have lowered the rate at which scaffolds absorb water. All samples absorbed twice their weight in PBS solution after immersion as shown in (Fig.4b) and summarized in Table 4. PCSG0.0 samples absorbed the most PBS, resulting in 128 % swelling. With the addition of GNSs, water absorption was slightly decreased. PCSG10.0 also had a lower swelling percentage of 115% compared to PCSG0.0. The presence of GNS seems to lower the amount of PBS absorbed.

	W_i (g)	W_f (g)	$W_{swelling}$ %	±
PCSG0.0	0.0306	0.0707	128%	6%
PCSG10.0	0.0041	0.0091	115%	6%

Table 4. Percent swelling of PCSG scaffolds after immersion in PBS.

Since fewer hydrophilic sites are available to bind water when GNS concentration rises, less water is absorbed, and swelling is reduced (Cheng *et al.*, 2018; Shin *et al.*, 2016; Zhang *et al.*, 2016). Thus, hydrophilicity/hydrophobicity must be carefully controlled to balance water uptake and swelling benefits with hazards of excessive water uptake. Swelling can also cause scaffold degradation, mechanical weakness, and instability. It can also result in the loosening of the scaffold from its implant and the generation of unnecessary stress on surrounding tissues (Chung *et al.*, 2022). The phenomenon is due to the polymer chains in a scaffold swelling and stretching as they absorb fluid, thereby widening the space between the chains. As a result, the intermolecular forces that keep the chains together are weakened which lowers the scaffold's stiffness and strength. With the presence of GNSs, swelling is reduced as they obstruct chain-scale polymer center-of-mass diffusion when they are present in a polymer matrix (Bailey & Winey, 2020). GNSs create defects in the polymer chains that serve as physical obstacles that may obstruct water penetration (Bailey & Winey, 2020). Controlling a scaffold's level of water absorption is crucial. The scaffold may enlarge, deteriorate, and lose its mechanical qualities if it absorbs too much water. However, if the scaffold does not absorb enough water, *in vitro*, it may impede cell migration and growth and restrict the movement of nutrients and waste.

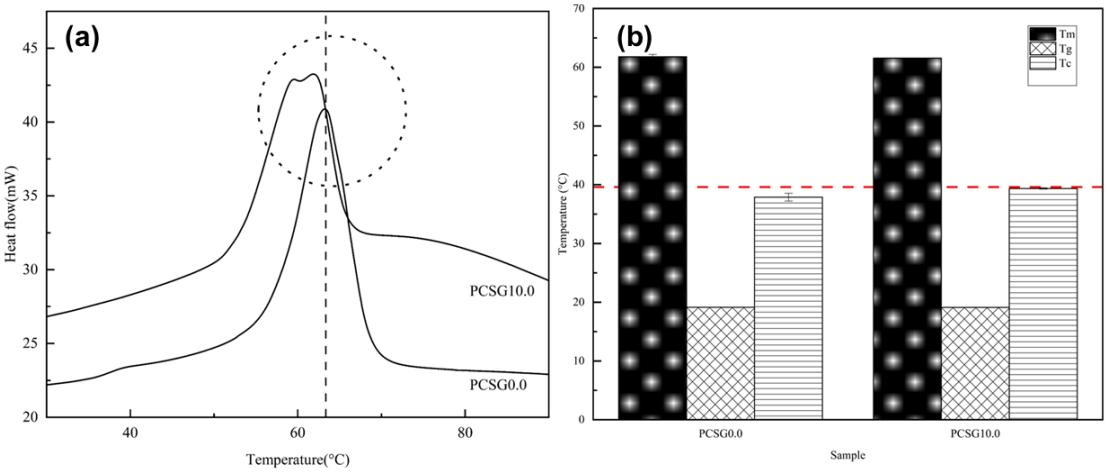

Figure 5. a) DSC thermograms as a function of PCSG scaffolds, b) melting temperature, glass transition temperature, and crystallization temperature PCSG scaffolds.

Fig. 5a shows the representative DSC traces of PCL/CHT and its GNS nanocomposites. Distinct endothermic melting peaks (T_m) at 61.8, and 61.6 ºC for PCSG0.0, and PCSG10.0, respectively, were observed, suggesting no significant change in the melting temperature. This could be due to the low amount of the nanofiller used to make the nanocomposites. Another observation made was that the melting peak shifts to the left and splits into two peaks. This means that the polymer melts at a lower temperature with two melting regions. The reason for this effect is that GNS can act as nucleating agents for polymer crystallization and can promote the formation of ordered structures in a material also due to phase transition (Ajala *et al.*, 2019; Chung *et al.*, 2022). When GNS is well

dispersed in the polymer matrix, it can provide sites for the polymer chains to align and crystallize around them (Ajala *et al.*, 2019). This increases the energy required for the polymer to melt and raises the melting temperature. However, not all polymer chains can crystallize around GNS. Some chains may remain amorphous or have less ordered structures(Svoboda & Málek, 2011). These chains have weaker intermolecular forces and melt at a lower temperature than the crystalline chains (Svoboda & Málek, 2011). Therefore, the polymer matrix has two melting regions: one for the crystalline chains and one for the amorphous or less ordered chains (Blundell, 1987). Due to the low concentration of GNSs used in this study, the effect is not significant therefore the change in melting temperature is not significant.

A slight change of Tc is noticed from 37.9, and 39.4 ºC for PCSG0.0, and PCSG10.0, respectively, suggesting a change in the crystalline structure. This is due to the nucleating effect of GNSs on PCSG crystallization. Similarly, polymer chains may also align due to nucleation effect of GNSs, which increases the crystallization behavior of nanocomposites. GNSs increase the crystallization temperature and broaden the crystallization peak, indicating restricted mobility of polymer chains in the nanocomposite. The glass transition temperature Tg was insignificantly different as shown in (Fig. 5b) with values of 19.14 and 19.13 ºC for PCSG0.0 and PCSG10.0 respectively suggesting no change in the chemical structure as corroborated in the FTIR analysis. T_m values were all within a relatively small range (61.6-61.8 ºC), which also indicates that the addition of GNSs did not significantly change the melting behavior of the polymer matrix. The enthalpy of fusion was decreased from 65.3 (J/g) in PCSG0.0 to 51.8 (J/g) in PCSG10.0, indicating that GNS might act as a nucleating agent and may reduce the crystallinity of the polymers due to the strong interfacial interactions between them. GNS has high surface area and with wrinkled yet scrolled morphology, they can induce strong interactions with the macromolecular chain leading to reduced chain flexibility, resulting in lower ability to crystallize. However, we have two polymer systems (PCL and CHT), with PCL having higher crystallization capability. So, the overall effect resulted into a slight increase in the Tc, while a slight decrease in Tm and enthalpy of fusion.

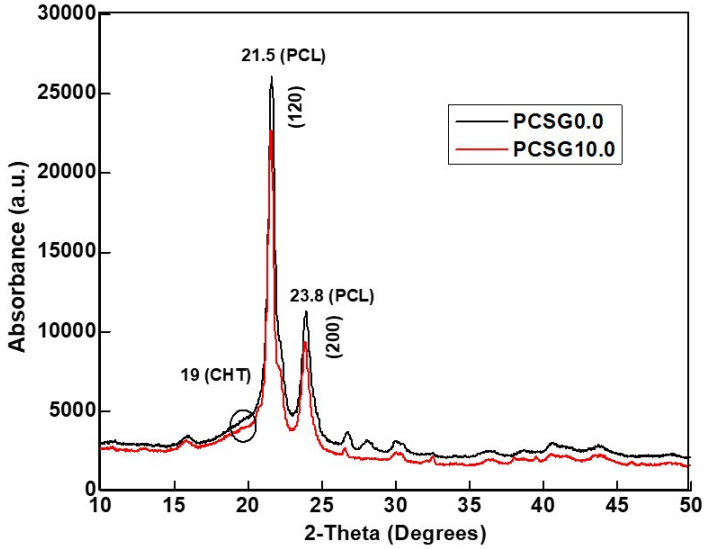

Figure 6. X-ray diffraction (XRD) spectra of PCSG scaffolds.

The XRD patterns of the PCSG scaffolds (Fig. 6) show two prominent peaks at 21.5 and 23.8º, owing to the (120), and (200) crystal planes of PCL. These peaks indicate the presence of well-ordered crystalline regions within the PCL component of the composite. The absence of any detectable peaks for CHT suggests that it has an exceptionally low degree of crystallinity, in addition to the low concentrations of CHT used in this study. This is expected, as CHT is known to have a more amorphous structure compared to PCL. The amorphousness is due to its branched structure and the presence of many bulky side groups that disrupt the formation of ordered crystals.

The addition of GNS to the PCL-CHT composite is expected to influence the crystalline structure of PCL. The increase in GNS concentration led to GNS acting as nucleation sites for PCL crystallization, leading to an increase in the overall crystallinity of the composite (Wu *et al.*, 2011) (shown in Table 1, the PCSG10.0 scaffold exhibited the highest crystallinity of 61.1%. The PCSG0.0 scaffold had a crystallinity of 58.6%. The increase in crystallinity with the addition of GNSs can be attributed to the nucleation effect of the GNS on the PCL/CHT matrix. GNSs act as nucleation sites for the PCL/CHT chains to crystallize around, leading to an increase in the number of crystalline domains and thus the overall crystallinity of the scaffold. The higher concentration of GNS (0.1 wt.%) resulted in a greater nucleation effect, leading to a higher crystallinity of 61%. Overall, the XRD results corroborate the DSC results confirming that the addition of GNS to PCL/CHT scaffolds can increase their crystallinity and thus potentially improve their mechanical properties.

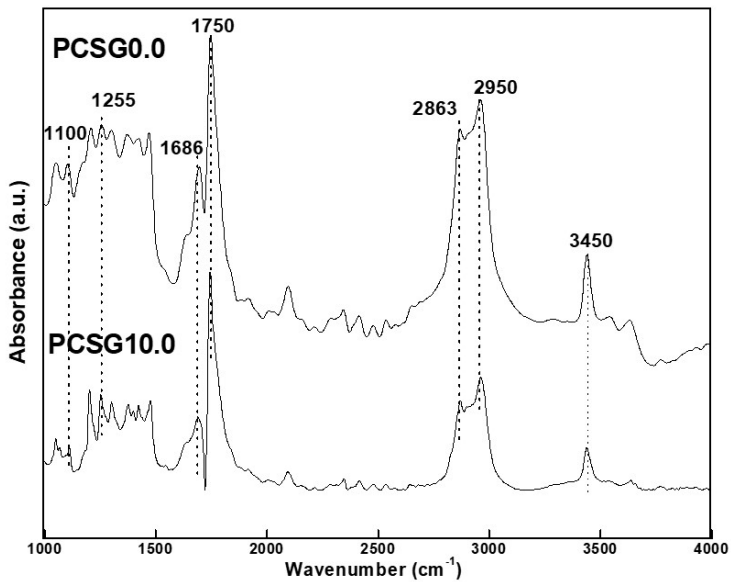

Figure 7. FTIR spectra of PCSG0.0 and PCSG10.0 scaffolds.

FTIR spectroscopy analysis was used to assess the chemical composition of the scaffolds before and after *in vitro* enzymatic degradation. As shown in (Fig. 7), the characteristic peaks of CHT, which were observed at 3450, 2863, 1686, and 1100 cm^{-1}, were attributed to the stretching vibrations of the intramolecular hydrogen bonding of -NH_2 and -OH groups, -CH- and -CH_2-, amide I, amide II, and C-O, respectively (Das *et al.*, 2019, 2020). The typical peaks for C-H and ester carbonyl (C=O) groups from PCL at 2950 and 1750 cm^{-1} are also observed(Das *et al.*, 2020). No new peaks were observed suggesting no covalent interactions between the polymers. A low concentration of GNS also did not impart any significant changes in the FTIR spectra.

Now we discuss the enzymatic degradation of PCL-CHT scaffolds (without GNS) using the FTIR spectra of these scaffolds. As shown in (Fig. 8a), the peaks of the symmetric stretching vibration and the asymmetric stretching vibration of methyl groups were observed at 2950 cm^{-1} and 2863 cm^{-1}, respectively. Over the course of 3 weeks of enzymatic degradation, it was observed that the peak due to the C-H group's asymmetric bending of CHT (2863 cm^{-1}) diminished steadily throughout degradation in all samples and almost disappeared after 2-3 weeks of enzymatic degradation. This indicates that the degradation process is causing the cleavage of the ester bonds in the PCL and CHT components of the composite, leading to a decrease in the number of CH_2 groups and an increase in the number of carbonyl groups in the structure. A high-intensity peak at 1255 cm^{-1}, due to the asymmetric elongation of C-O-C, decreased steadily due to degradation. (Fig. 8b) shows the FTIR spectra in the 1800-1650 cm^{-1} region. PCL-CHT scaffolds exhibited a broad peak at 1750 cm^{-1} (C=O stretching vibration of ester), while bands at 1722 cm^{-1} (crystalline phase of PCL) and a band at 1165 cm^{-1} (circled in Fig. 8a)

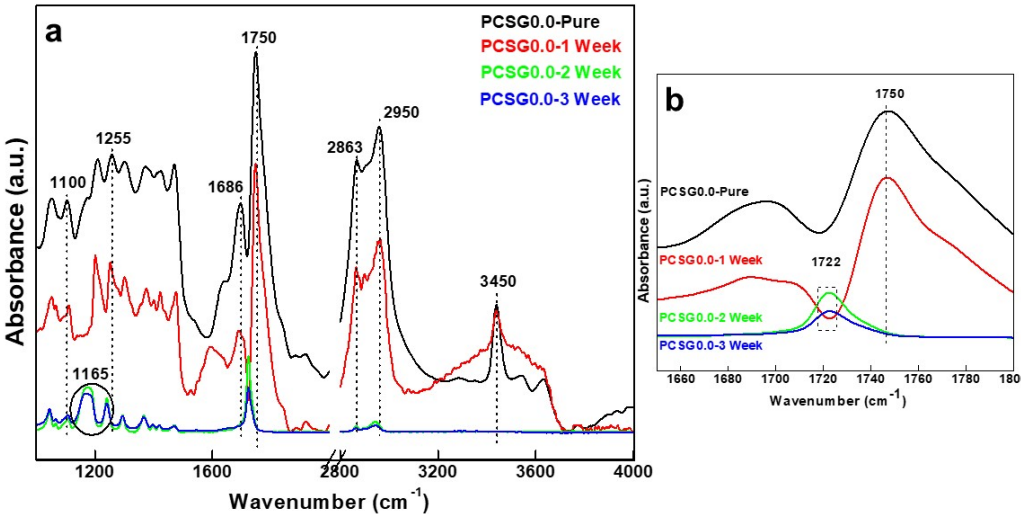

Figure 8. FTIR spectra of scaffolds after enzymatic degradation of PCSG0.0 scaffolds. a) full range spectrum, while b) spectra in the range of 1800-1600 cm^{-1}.

assigned to stretching vibration of C-O bond, which is associated with the amorphous region of PCL. This data suggests that with increasing degradation time (2-3 weeks), the CHT component is primarily degraded, exposing the crystalline and amorphous regions of PCL. Further, the peaks associated with N-H and O-H stretching vibrations decrease in intensity during degradation, indicating the breakdown of the polymer chains due to the deacetylation of CHT (Das *et al.*, 2020). The noticeable trend emerges as the major peaks in the absorbance spectra exhibit a consistent and gradual decrease.

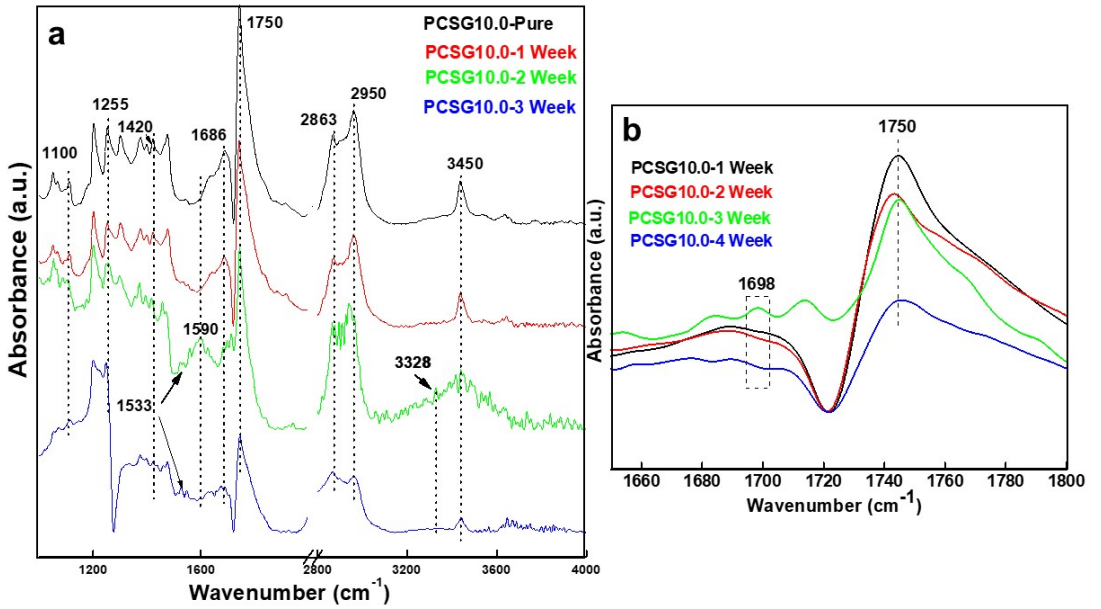

Figure 9. FTIR spectra of scaffolds after enzymatic degradation of PCSG10.0 scaffolds. a) full range spectrum, while b) spectra in the range of 1800-1600 cm 1.

In contrast to the behavior of pure PCL-CHT scaffolds, the FTIR spectra of PCL-CHT-GNS scaffolds after 2 and 3 weeks were similar to pure undegraded sample and no significant changes were observed, suggesting the role of GNS to control/mitigate the degradation of PCL-CHT (Fig. 9). Our results further validates that the incorporation of GNS in polymer matrices is responsible for the stability

and hence delayed degradation of CHT and PCL. Further, GNS can not only create a tortuous path for the influx of enzymes and outflux of degradation products but can also make the matric structurally stable and physically robust such that the macromolecular chains are closely packed. These unique features of GNS render the scaffolds physically stable and less vulnerable to early degradation. This is preferred because 1-4 weeks are considered short for adequate tissue growth. Moreover, the peaks at 3328 cm^{-1} and 1533 cm^{-1} (Fig. 9a) are assigned to the N-H bond in the NH_3^+ group in amino acids after 2-3 weeks of enzymatic hydrolysis, suggesting the adsorption of enzymes onto the rough surface of PCL-CHT-GNS nanohybrid scaffolds. This could be due to the scrolled architecture of GNS that assists in the immobilization of the enzymes into its lumen, thereby prolonging the degradation. A notable decline in the intensity of the peaks at 1750 cm^{-1} and 1698 cm^{-1} (Fig. 9b), associated with the C=O stretching vibrations of ester groups, is apparent. This reduction in intensity may also be ascribed to the steady enzymatic hydrolysis of the ester bonds.

Nanofillers can slow the degradation process or inhibit the onset of degradation by immobilizing the polymer or free radical chains and by delaying the evolution of the degradation products from the respective samples (Luyt & Kelnar, 2019). In this study, a steady decrease in absorbance was observed in PCSG0.0 compared to PCSG10.0 over the 21 days for most of the peaks of CHT and PCL. The diminishing intensity of these peaks could indicate changes in the underlying molecular vibrations or compositions, linked to ongoing chemical reactions or structural modifications taking place over time. These observed patterns highlight the potential impact of the time under degradation on the absorbance spectra, underscoring the need for further investigation to elucidate the exact mechanisms driving this phenomenon and its broader implications.

The modulus for PCSG0.0 and PCSG10.0 samples were recorded as 0.55 (GPa) and 1.17 (GPa), respectively. The increase in Young's modulus (~110%) observed in PCSG scaffolds containing 0.1 wt.% GNS is likely due to the improved dispersion of the nanoscrolls in the polymer matrix, leading to more effective reinforcement and increased stiffness. On the other hand, a marginal increment in hardness was observed for PCSG10 samples (data not reported). The modulus of a scaffold affects its ability to deform and absorb mechanical loads, which is important for the successful growth and function of cells and tissues. If a scaffold has a high elastic modulus, it will be stiff and inflexible, which may cause damage to cells and tissues. On the other hand, if a scaffold has a low elastic modulus, it may not provide enough mechanical support to cells and tissues. Therefore, it is important to carefully control the elastic modulus of tissue engineering scaffolds to ensure that they provide appropriate mechanical support for cell and tissue growth while minimizing the risk of mechanical damage. This can be achieved through the optimization of scaffold design and fabrication methods, and the control of processing conditions.

CONCLUSION

Our data indicates that reinforcing PCL and CHT with GNSs, even at low concentrations of 0.1wt.%, resulting in a decrease in enzymatic degradation. The lower degradation is due to the tortuous path of dispersed GNS, making it challenging for enzymes to reach the bulk matrix. When GNSs are present in the polymer matrix, they hinder the diffusion of the polymer chains, as they create defects that act as physical barriers to water penetration which results in less swelling. In the presence of GNS, the crystallization temperature rises, and the crystallization peak broadens, indicating restricted polymer chain mobility within the nanocomposite. GNS can act as nucleation sites for PCL crystallization, thereby increasing the composite's overall crystallinity demonstrated in this study that an optimal GNS content can improve mechanical properties without altering the chemical structure of the scaffold. To noticeably improve the biocompatibility and mechanical properties such as modulus and hardness, in-depth investigation may be beneficial to ascertain a suitable GNS amount for tissue engineering applications.

Acknowledgment

This research was supported by the Louisiana Board of Regents Support Fund, RCS project, contract number LEQSF (2020-23)-RD-A-21.

Conflict of interest

The authors declare that they have no known competing financial interests or personal relationships that could have any influence on the work reported in this paper. ♦

REFERENCES

Abdelfatah, J., Paz, R., Alemán-Domínguez, M. E., Monzón, M., Donate, R., & Winter, G. (2021). Experimental Analysis of the Enzymatic Degradation of Polycaprolactone: Microcrystalline Cellulose Composites and Numerical Method for the Prediction of the Degraded Geometry. *Materials, 14*(9), 2460. https://doi.org/10.3390/ma14092460

Ajala, O., Werther, C., Nikaeen, P., Singh, R. P., & Depan, D. (2019). Influence of graphene nanoscrolls on the crystallization behavior and nano-mechanical properties of polylactic acid. *Polymers for Advanced Technologies, 30*(7), 1825-1835. https://doi.org/10.1002/pat.4615

Aranaz, I., Alcántara, A. R., Civera, M. C., Arias, C., Elorza, B., Heras Caballero, A., & Acosta, N. (2021). Chitosan: An Overview of Its Properties and Applications. *Polymers, 13*(19), 3256. https://doi.org/10.3390/polym13193256

Ashammakhi, N., GhavamiNejad, A., Tutar, R., Fricker, A., Roy, I., Chatzistavrou, X., Hoque Apu, E., Nguyen, K.-L., Ahsan, T., Pountos, I., & Caterson, E. J. (2022). Highlights on Advancing Frontiers in Tissue Engineering. *Tissue Engineering Part B: Reviews, 28*(3), 633-664. https://doi.org/10.1089/ten.teb.2021.0012

Bailey, E. J., & Winey, K. I. (2020). Dynamics of polymer segments, polymer chains, and nanoparticles in polymer nanocomposite melts A review. *Progress in Polymer Science, 105*, 101242. https://doi.org/10.1016/j.progpolymsci.2020.101242

Bartnikowski, M., Dargaville, T. R., Ivanovski, S., & Hutmacher, D. W. (2019). Degradation mechanisms of polycaprolactone in the context of chemistry, geometry, and environment. *Progress in Polymer Science, 96*, 1-20. https://doi.org/10.1016/j.progpolymsci.2019.05.004

Basavegowda, N., & Baek, K.-H. (2021). Advances in Functional Biopolymer-Based Nanocomposites for Active Food Packaging Applications. *Polymers, 13*(23), 4198. https://doi.org/10.3390/polym13234198

Biscaia, S., Silva, J. C., Moura, C., Viana, T., Tojeira, A., Mitchell, G. R., Pascoal-Faria, P., Ferreira, F. C., & Alves, N. (2022). Additive Manufactured Poly (ε-caprolactone)-graphene Scaffolds: Lamellar Crystal Orientation, Mechanical Properties and Biological Performance. *Polymers, 14*(9), 1669. https://doi.org/10.3390/polym14091669

Blundell, D. J. (1987). On the interpretation of multiple melting peaks in poly(ether ether ketone). *Polymer, 28*(13), 2248-2251. https://doi.org/10.1016/0032-3861(87)90382-X

Bonithon, R., Kao, A. P., Fernández, M. P., Dunlop, J. N., Blunn, G. W., Witte, F., & Tozzi, G. (2021). Multi-scale mechanical and morphological characterization of sintered porous magnesium-based scaffolds for bone regeneration in critical-sized defects. *Acta Biomaterialia, 127*, 338-352. https://doi.org/10.1016/j.actbio.2021.03.068

Castilla-Cortázar, Vidaurre, Marí, & Campillo-Fernández. (2019). Morphology, Crystallinity, and Molecular Weight of Poly(ε-caprolactone)/Graphene Oxide Hybrids. *Polymers, 11*(7), 1099. https://doi.org/10.3390/polym11071099

Cheng, X., Wan, Q., & Pei, X. (2018). Graphene Family Materials in Bone Tissue Regeneration: Perspectives and Challenges. *Nanoscale Research Letters, 13*(1), 289. https://doi.org/10.1186/s11671-018-2694-z

Chung, J. H. Y., Sayyar, S., & Wallace, G. G. (2022). Effect of Graphene Addition on Polycaprolactone Scaffolds Fabricated Using Melt-Electrowriting. *Polymers, 14*(2), 319. https://doi.org/10.3390/polym14020319

Das, P., Remigy, J.-C., Lahitte, J.-F., van der Meer, A. D., Garmy-Susini, B., Coetsier, C., Desclaux, S., & Bacchin, P. (2020). Development of double porous poly (ε - caprolactone)/chitosan polymer as tissue engineering scaffold. *Materials Science and Engineering: C, 107*, 110257. https://doi.org/10.1016/j.msec.2019.110257

Das, P., Salerno, S., Remigy, J.-C., Lahitte, J.-F., Bacchin, P., & De Bartolo, L. (2019). Double porous poly (Ɛ-caprolactone)/chitosan membrane scaffolds as niches for human mesenchymal stem cells. *Colloids and Surfaces B: Biointerfaces, 184*, 110493. https://doi.org/10.1016/j.colsurfb.2019.110493

Depan, D., Venkata Surya, P. K. C., Girase, B., & Misra, R. D. K. (2011). Organic/inorganic hybrid network structure nanocomposite scaffolds based on grafted chitosan for tissue engineering. *Acta Biomaterialia, 7*(5), 2163-2175. https://doi.org/10.1016/j.actbio.2011.01.029

Ferroni, L., Gardin, C., Rigoni, F., Balliana, E., Zanotti, F., Scatto, M., Riello, P., & Zavan, B. (2022). The Impact of Graphene Oxide on Polycaprolactone PCL Surfaces: Antimicrobial Activity and Osteogenic Differentiation of Mesenchymal Stem Cell. *Coatings, 12*(6), 799. https://doi.org/10.3390/coatings12060799

Islam, Md. M., Shahruzzaman, Md., Biswas, S., Nurus Sakib, Md., & Rashid, T. U. (2020). Chitosan based

bioactive materials in tissue engineering applications-A review. *Bioactive Materials, 5*(1), 164-183. https://doi.org/10.1016/j.bioactmat.2020.01.012

Kao, H.-H., Kuo, C.-Y., Tagadur Govindaraju, D., Chen, K.-S., & Chen, J.-P. (2022). Polycaprolactone/Chitosan Composite Nanofiber Membrane as a Preferred Scaffold for the Culture of Mesothelial Cells and the Repair of Damaged Mesothelium. *International Journal of Molecular Sciences, 23*(17), 9517. https://doi.org/10.3390/ijms23179517

Kean, T., & Thanou, M. (2010). Biodegradation, biodistribution and toxicity of chitosan. *Advanced Drug Delivery Reviews, 62*(1), 3-11. https://doi.org/10.1016/j.addr.2009.09.004

Lanjewar, S., Mukherjee, A., Rehman, L., Abdelrasoul, A., & Roy, A. (2020). Thermodynamics of Casting Solution in Membrane Synthesis. In *Modeling in Membranes and Membrane-Based Processes* (pp. 9-45). Wiley. https://doi.org/10.1002/9781119536260.ch2

Loh, Q. L., & Choong, C. (2013). Three-Dimensional Scaffolds for Tissue Engineering Applications: Role of Porosity and Pore Size. *Tissue Engineering Part B: Reviews, 19*(6), 485-502. https://doi.org/10.1089/ten.teb.2012.0437

Luyt, A. S., & Kelnar, I. (2019). Effect of blend ratio and nanofiller localization on the thermal degradation of graphite nanoplatelets-modified PLA/PCL. *Journal of Thermal Analysis and Calorimetry, 136*(6), 2373-2382. https://doi.org/10.1007/s10973-018-7870-y

Matsuda, S. (1991). Thermodynamics of Formation of Porous Polymeric Membrane from Solutions. *Polymer Journal, 23*(5), 435-444. https://doi.org/10.1295/polymj.23.435

Mondal, D., Griffith, M., & Venkatraman, S. S. (2016). Polycaprolactone-based biomaterials for tissue engineering and drug delivery: Current scenario and challenges. *International Journal of Polymeric Materials and Polymeric Biomaterials, 65*(5), 255-265. https://doi.org/10.1080/00914037.2015.1103241

Parisien, A., ElSayed, M. S. A., & Frei, H. (2022). Mature bone mechanoregulation modelling for the characterization of the osseointegration performance of periodic cellular solids. Materialia, 25, 101552. https://doi.org/10.1016/j.mtla.2022.101552

Shin, S. R., Li, Y.-C., Jang, H. L., Khoshakhlagh, P., Akbari, M., Nasajpour, A., Zhang, Y. S., Tamayol, A., & Khademhosseini, A. (2016). Graphene-based materials for tissue engineering. *Advanced Drug Delivery Reviews, 105*, 255-274. https://doi.org/10.1016/j.addr.2016.03.007

Sun, R., Chen, H., Sutrisno, L., Kawazoe, N., & Chen, G. (2021). Nanomaterials and their composite scaffolds for photothermal therapy and tissue engineering applications. *Science and Technology of Advanced Materials, 22*(1), 404-428. https://doi.org/10.1080/14686996.2021.1924044

Svoboda, R., & Málek, J. (2011). Interpretation of crystallization kinetics results provided by DSC. *Thermochimica Acta, 526*(1-2), 237-251. https://doi.org/10.1016/j.tca.2011.10.005

Wu, D., Lin, D., Zhang, J., Zhou, W., Zhang, M., Zhang, Y., Wang, D., & Lin, B. (2011). Selective Localization of Nanofillers: Effect on Morphology and Crystallization of PLA/PCL Blends. *Macromolecular Chemistry and Physics, 212*(6), 613-626. https://doi.org/10.1002/macp.201000579

Zhang, B., Wei, P., Zhou, Z., & Wei, T. (2016). Interactions of graphene with mammalian cells: Molecular mechanisms and biomedical insights. *Advanced Drug Delivery Reviews, 105*, 145-162. https://doi.org/10.1016/j.addr.2016.08.009